IRAQI JOURNAL OF MATERIALS
Volume (3) Issue (4) October-December 2024, pp. 39-44

Characterization of Indium Nitride Thin Films Prepared by Plasma-Assisted Molecular Beam Epitaxy

Ali M. Hassan [1], Peter M. Millner [2], James G. McAlley [2]

[1] *Department of Medical Physics, Al-Hasseb University College, Najaf, IRAQ*
[2] *Department of Physics, Faculty of Science, Bournemouth University, Bournemouth, UK*

Abstract

The growth and electronic structure of indium nitride has been presented. Indium nitride thin films were grown by plasma-assisted molecular beam epitaxy (PAMBE). The significance of the relative fluxes, substrate temperature and buffer layers was explored and related to the electrical and structural properties of the prepared films. Alongside the effect of active nitrogen species on indium nitride films, it was found that excited molecular nitrogen was preferred for growth over atomic and ionic species. An optimized recipe for indium nitride was developed incorporating all explored parameters.

Keywords: Indium nitride; Molecular beam epitaxy; Thin films; Electronic structure
Received: 20 April 2024; **Revised:** 22 July 2024; **Accepted:** 29 July 2024; **Published:** 1 October 2024

1. Introduction

Epitaxy is defined as the deposition of a monocrystalline film on a monocrystalline substrate, keeping a certain lattice alignment known as epitaxial relationship. The heteroepitaxy is used when the substrate and the epilayer are different materials [1,2]. Heteroepitaxy is the deposition of material A on material B. In this case, various growth modes can be observed, depending on the lattice mismatch between the materials and surface energy: Layer-by-layer growth, also called Frank Van der Merwe growth, Three-dimensional (3D) growth, called Volmer-Weber growth, and Stranski-Krastanov growth [3-5]

High quality epitaxial thin films can be synthesized via chemical vapor deposition (CVD) or physical deposition (Molecular Beam Epitaxy, MBE) [6,7]. In comparison to CVD techniques, MBE presents several advantages which stem from its lower growth temperature and in situ monitoring via Reflection High-Energy Electron Diffraction (RHEED) [8,9]. They are good control of layer thickness, due to a low growth rate (less than one monolayer (ML) per second) and reduced inter-diffusion effects [10]. Also, synthesis of a wide range of ternary or quaternary alloys. Even materials that are barely miscible under thermodynamic equilibrium can be dynamically stabilized by MBE [11]. Finally, higher dopant concentrations thanks to the minimization of segregation effects [12].

In the particular case of III-nitrides, additional advantages can be found, such as the possibility to change the material polarity, depending on the substrate or buffer layer [13,14]. As well, the activation of Mg-dopant is not required, because of the H-free growth environment [15].

The epitaxial growth process depends on the impinging fluxes on the one hand and the substrate temperature on the other hand [16]. The substrate temperature is the key parameter which activates the different phenomena occurring at the growing surface [17].

As can be seen in Fig. (1), the impinging fluxes can be adsorbed at the surface by chemisorption (if chemical bonds are created via a transfer of electrons between impinging atoms and atoms from the surface) or physisorption (if the atoms are adsorbed via Van der Waals forces) [18]. At a given substrate temperature and concentration, the atoms have a certain mobility [19]. Some of the species will diffuse and be desorbed without being incorporated to the layer, whereas the others will incorporate either by step-edge growth forming atomic terraces or by cluster nucleation [20].

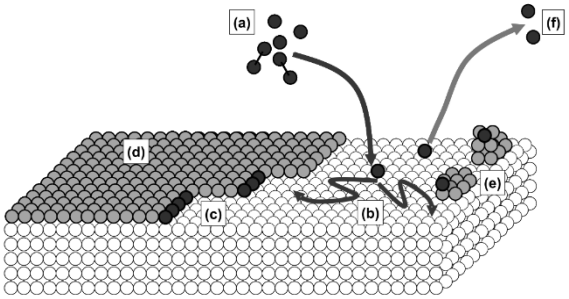

Fig. (1) Atomistic processes that can occur at the surface during the growth: (a) adsorption, (b) diffusion, (c) step-edge growth, (d) atomic terraces, (e) nucleation of clusters and (f) desorption

Techniques that have led to low cost, high density processing of silicon have resulted in silicon integrated circuits becoming ubiquitous within modern society. The astonishing progress which has been achieved in the processing of silicon is encompassed by Moore's law [21,22]. In 1965, only 5 years after the first planar integrated circuit was produced, Gordon Moore noted that the density of transistors being fabricated on silicon integrated circuits was doubling approximately every 2 years [23]. Remarkably this trend has continued to the present day and the latest generation of microprocessors now pack more than half a billion transistors onto a square centimeter [24,25].

While the ability of semiconductors to rapidly process information may be the most visible application, semiconductors are used in applications as wide reaching as solid state lighting, power distribution, photovoltaics and high speed communications [26-29]. When considering which semiconductor is preferred for a given application a number of material properties must be considered. High frequency devices rely on high peak carrier drift velocities along with compatibility with high-k dielectrics [30]. For light emitting applications, the size and nature of the electronic bandgap must be considered. High power operation requires the material to be relatively insensitive to moderate changes in temperature [31].

The first report of III-nitrides synthesis was in 1938 by Juza et al. who synthesized GaN and InN crystallites [32]. The GaN was formed by flowing ammonia over hot gallium, and the InN from $InF_6(NH_4)_3$ reduction. The purpose of this initial study was to measure lattice parameters of the materials and there was little interest in their optical properties at that stage [33]. It was 30 years later, when Maruska et al. first grew GaN layers by vapor phase deposition on sapphire substrates, that interest in the nitrides increased [34]. Following this report, blue LEDs based on GaN:Zn/n-GaN structures were produced by Pankove et al. on vapor phase grown GaN [35,36]. These structures relied on hot carrier injection from avalanche breakdown to generate holes. Despite subsequent advances in growth, p-type GaN proved elusive and it was not until 1989 when Amano et al. succeeded in reliably producing p-type GaN by Mg doping [37]. Nakamura et al. have utilized Mg doping to form p-n junctions, and at the time, the brightest blue LEDs made from any material system [38]. Akasaki et al. and Nakamura et al. subsequently produced the first laser diodes based on the material system [39,40]. Progress has continued at a remarkable rate, with the number of research groups studying the III-nitrides ballooning [41]. Recent efforts have focused on improving the efficiency of nitride based LEDs and laser diodes and extending the range of wavelengths over which they operate. Added effort has also been applied to HEMTs based on nitride heterojunctions [42]. For a thorough account of the historical developments in the GaN field see the reviews by Jain et al. [43] and Pankove et al. [44].

2. Experimental Work

The nitride MBE system used in this work is a Perkin-Elmer model 430. The water cooled chamber is fitted with ion and cryo pumps (cryo pumped exclusively during film growth) which results in a base pressure of about $5x10^{-11}$ Torr. Active nitrogen is supplied by a radio frequency inductively coupled plasma source, and all metallic species are supplied by standard or high temperature effusion cells. Samples can be transferred in and out of the system using a three chamber load-lock. Growth can be monitored in-situ by a reflection high energy electron diffraction (RHEED) system, and also a custom built laser interferometer. Substrates are mounted on 78 mm molybdenum blocks via indium or indium-tin solder. The growth temperature can be controlled by a high temperature substrate manipulator heater capable of temperatures greater than 1200°C. The substrate manipulator temperature is monitored by a thermocouple touching the back side of the molybdenum block. Growth temperatures were calibrated using a silicon/aluminum eutectic.

As the common form of nitrogen is inert at achievable growth temperatures, a plasma or ion source is required to activate the N_2 molecule. The primary source used in this work was an HD-25 radio frequency inductively coupled plasma source (RF-ICP). An earlier plasma source model, the MDP-21, was used for initial studies. Unless otherwise stated, results refer to growth with the HD-25. All nitrogen which flowed into the RF-ICP was filtered by a nickel inert gas filter, and flow was moderated by a 0-5 sccm mass flow controller. The basic structure of an RF-ICP is shown in Fig. (1).

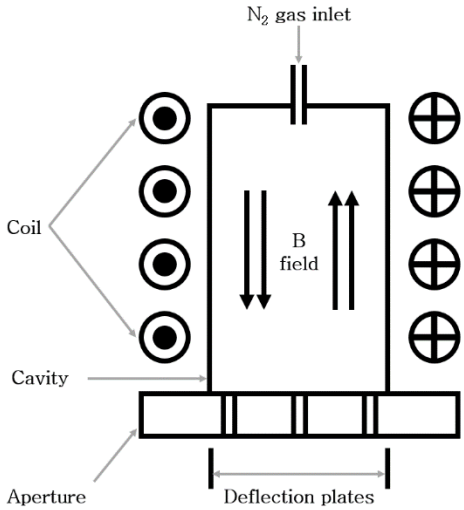

Fig. (1) The main features of a radio frequency inductively coupled plasma source

Nitrogen is controllably leaked into the cavity via the inlet. A water cooled coil couples the RF signal into the cavity via a magnetic field which is most intense at the center of the cavity. The alternating field accelerates charged particles which collide further with other species and a plasma is formed. Typically the source (both HD-25 and MDP-21) was operated at RF powers of 150-350 W and a flow rate of 1.3 sccm for film growths. The species generated by an RF-ICP can vary substantially at different plasma operating conditions and also from different source geometries.

A number of post growth characterization techniques are discussed within this chapter. It is not feasible to give a comprehensive overview of each technique, so only a brief technique summary is given here along with key operating parameters. The reader is directed to the thorough review of semiconductor characterization techniques [45] for further information.

3. Results and Discussion

In order to map out the different growth regimes for the MBE system, two GaN films were grown with the Ga flux varied in discreet steps. The nitrogen plasma conditions were unchanged during growth and the growth rate was measured at the various flux ratios by laser interferometry using a semiconductor laser operating at 658 nm. The films were both grown on sapphire substrates at 700°C with a low temperature GaN buffer grown at 500°C. Figure (2) shows the growth rate of the two GaN films grown at RF powers of 350 W and 150 W, respectively.

A constant nitrogen flow rate of 1.3 sccm was used for both films. As we can see from Fig. (3), no intermediate regime exists at growth temperatures of 700°C. This indicates that the saturation in growth rate in both figures (2a) and (2b) marks the transition between N-rich and Ga-rich conditions. Increasing the RF power shifts the transition between the two regimes to higher Ga flux. By using these plots it was possible to choose a Ga flux that was slightly into the Ga-rich regime. This corresponded to a Ga flux of 2.1 and 1.5×10^{14} atoms/cm^2.s for the 350 and 150 W plasma measurements, respectively. This Ga flux was then used for future optimized GaN films and buffer layers. It should be noted that the laser interferometry technique became available only towards the end of this thesis and originally the transition to the Ga-rich regime had been determined by observing the presence of Ga droplets on film surfaces. This original approach yielded a Ga flux within 5% of the laser interferometry determined Ga flux for the boundary between the two regimes.

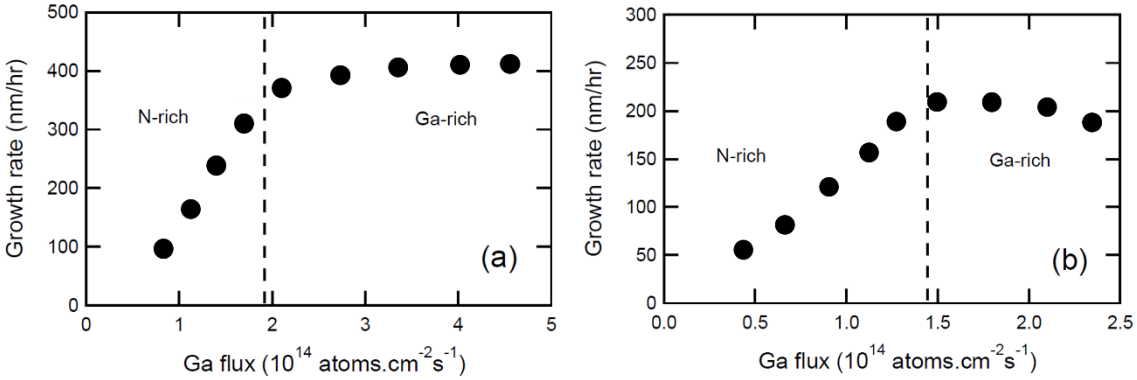

Fig. (2) The growth rate of GaN layers at various Ga fluxes. (a) Ga-polar GaN with plasma RF power of 350 W and flow rate of 1.3 sccm. (b) N-polar GaN with plasma RF power of 150 W and flow rate of 1.3 sccm. The dashed line represents the Ga flux where the growth rate begins to saturate, this point marks the transition between the N-rich and Ga-rich regimes

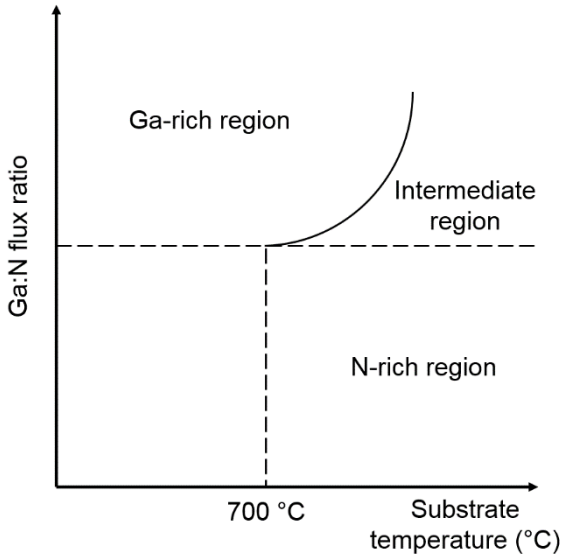

Fig. (3) The GaN growth diagram indicating the three conditions which MBE grown GaN can be produced

The polarity of GaN films has been shown to strongly influence film properties. Typically GaN films grown on sapphire by MBE are N-polar, while films grown on sapphire by MOCVD are Ga-polar. The Ga-polar surface has been shown to be the preferred surface for high quality GaN growth [46,47]. Often AlN buffer layers are employed to achieve the Ga-polar growth mode in MBE growth [48]. The other common technique used to achieve Ga-polar growth by MBE is to use an MOCVD grown GaN template as the substrate. In this work GaN layers were grown on sapphire and MOCVD GaN templates to achieve N-polar and Ga-polar layers, respectively. Films were grown on both substrates under Ga-rich and N-rich flux conditions. No nitridation step was used. Films had a 50 nm low temperature buffer layer grown at 500°C, and then a 400 nm high temperature layer grown at 700°C. Figure (4) shows AFM images of the four films, along with the root mean square (rms) roughness of each film.

Clearly the films grown on the GaN templates have much flatter morphologies, a result of the films growing homoepitaxially on an already relaxed GaN template. The films grown on sapphire, on the other hand, are highly strained due to the large lattice mismatch of GaN on sapphire. Additionally, the films grown on sapphire are expected to be N-polar as opposed to the preferred Ga-polarity of the MOCVD templates. The films grown in the Ga-rich regime show a small improvement in surface roughness, although the effect is small compared to the effect of the polarity and lattice mismatch.

From an InN perspective, the interest in GaN growth extends only as far as it can assist in producing improved InN films. As a buffer layer for InN, the GaN must be of high structural quality, indicating that growth in the Ga-rich regime with Ga-polarity should be preferred. We also want the GaN to be as electrically insulating as possible so that the buffer layers do not distort electrical measurements we

make on InN layers. Hall effect measurements on all GaN films revealed that the GaN layers had high resistivity. It was often difficult to obtain reliable Hall data as the currents achieved through the GaN layers were small. Carrier concentrations below 10^{18} cm^{-3} were common. Hall mobilities <10 $cm^2/V.s$ were measured for non-optimized films, and up to 150 $cm^2/V.s$ for optimized growth.

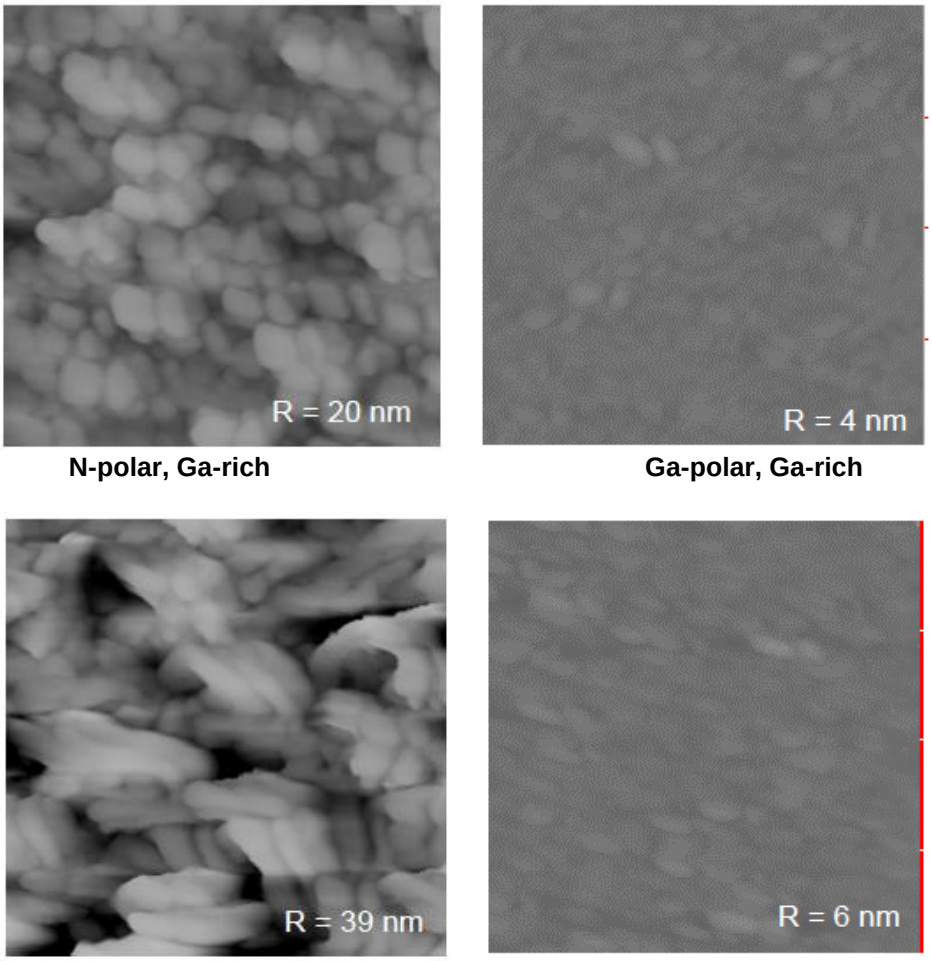

N-polar, Ga-rich **Ga-polar, Ga-rich**

N-polar, N-rich **Ga-polar, N-rich**

Fig. (4) AFM images of N-polar and Ga-polar GaN films grown in both the Ga-rich and N-rich regimes. R is the root mean square surface roughness

4. Conclusions

Indium nitride has been a very challenging material to grow with structural and electrical characteristics considered “high quality” by the electronics community. In particular, the limitations on growth temperature imposed by the dissociation of the material is a major hinderance. The growth regimes of the material were found to follow similar trends to the closely related GaN material system, with growth close to the “In-rich” regime preferred over growth at low In:N ratios.

References

[1] E.G. Bauer et al., “Fundamental issues in heteroepitaxy — A Department of Energy, Council on Materials Science Panel Report”, J. Mater. Res., 5 (1190) 85.
[2] M. Ohring, **“The Materials Science of Thin Films”**, Academic Press (San Diego, 1992) 197.
[3] T.K. Chu and A. Martinez, “Epitaxial IV-VI Semiconductor Films”, MRS Online Proc. Lib, 90 (1986) 59.
[4] J. Jacob et al., “Correlating in situ RHEED and XRD to study growth dynamics of polytypism in nanowires”, Nanoscale, 13 (2021) 13095-13107.
[5] D.S. McPhail, “Applications of Secondary Ion Mass Spectrometry (SIMS) in Materials Science”, J. Mater Sci., 41 (2006) 873-903.
[6] C. Lamberti, “The use of synchrotron radiation techniques in the characterization of strained semiconductor heterostructures and thin films”, Surf. Sci. Rep., 53(1-5) (2004) 1-197.
[7] G. Li and C. Jagadish, “Recent progress in δ-doping of III–V semiconductors grown by metal organic vapour phase epitaxy”, Sol. Stat. Electron., 41(9) (1997) 1207-1225.
[8] S. Angizi et al., “A comprehensive review on planar boron nitride nanomaterials: From 2D nanosheets towards 0D quantum dots”, Prog. Mater. Sci., 124 (2022) 100884.

 ISSN (print) 2958-8960 (online) xxxx-xxxx Printed in IRAQ

[9] L.-Q. Chen and Y. Zhao, "From classical thermodynamics to phase-field method", Prog. Mater. Sci., 124 (2022) 100868.
[10] C. Garlisi et al., "Multilayer thin film structures for multifunctional glass: Self-cleaning, antireflective and energy-saving properties", Appl. Ener., 264 (2020) 114697.
[11] L.A. Walsh et al., "Molecular Beam Epitaxy of Transition Metal Dichalcogenides" in **Molecular Beam Epitaxy**, 2nd ed., M. Henini (ed.) (2018) Ch. 22, 515-531.
[12] N.E. Richey, C. de Paula and S.F. bent, "Understanding chemical and physical mechanisms in atomic layer deposition", J. Chem. Phys., 152 (2020) 040902.
[13] J. Zúñiga-Pérez et al., "Polarity in GaN and ZnO: Theory, measurement, growth, and devices", Appl. Phys. Rev., 3 (2016) 041303.
[14] T.F. Kuech, S.E. Babcock and L. Mawst, "Growth far from equilibrium: Examples from III-V semiconductors", Appl. Phys. Rev., 3 (2016) 0404801.
[15] J.J. Meindl, "Beyond Moore's Law: the interconnect era", Comput. Sci. Eng., 5(1) (2003) 20-24.
[16] A.A. Demkov et al., "Materials for emergent silicon-integrated optical computing", J. Appl. Phys., 130 (2021) 070907.
[17] A. Yu, "The Future of Microprocessors", IEEE Micro, 16(6) (1996) 46-53.
[18] P. Zhang et al., "100 years of the physics of diodes", Appl. Phys. Rev., 4 (2017) 011304.
[19] T.Y. Kim, W. Suh and U. Jeong, "Approaches to deformable physical sensors: Electronic versus iontronic", Mater. Sci. Eng.: R: Reports, 146 (2021) 100640.
[20] A. Talaat et al., "Review on soft magnetic metal and inorganic oxide nanocomposites for power applications", J. Alloys Comp., 870 (2021) 159500.
[21] A. Balmer et al. "Oxide-defined GaSb VCSELs on ITO substrates", *J. Photon. Technol.*, 11 (1999) 33-36.
[22] C. Dwight et al. "Integration of III-V optoelectronic devices with Si-based circuitry", *Opt. Res. Lett.*, 13 (2001) 55-56.
[23] E. Fowler et al. "Bubble-Free Germanium Wafer Bonding in a Non-Cleanroom Ambient", *Czech J. Phys.*, 15 (2003) 67-70.
[24] G. Heinrisch et al. "Nickel contamination and indium segregation in directly bonded silicon wafers", *J. Solid Stat. Opt.*, 17 (2005) 81-84.
[25] I. Jafaar et al. "Bonding of silicon wafer by novel design of monolayers", *Acta Mater.*, 10 (2007) 103-106.
[26] K. Lancer et al. "Surface activation of silicon wafer bonding at low temperatures", *Mater. Commun.*, 12 (2009) 21-24.
[27] M. Neumann et al. "Room-temperature semiconducting wafer bonding in high vacuum environment", *J. Solid Stat. Technol.*, 8 (2012) 39-42.
[28] O. Parker et al. "Fusion bonding of oxidized silicon wafers at low temperatures", *Solid Stat. Lett.*, 14 (2015) 57-60.
[29] Q. Ronahi et al. "Fusion bonding of silicon wafers in low vacuum", *Solid Stat. Lett.*, 15 (2016) 113-116.
[30] S. Tucker et al. "Fusion bonding of silicon wafers with polymer thin films at room temperature", *Acta Mater.*, 13 (2010) 207-210.
[31] U. Vlahovich et al. "Low-dark-current wafer-bonded Si/InSb photodiodes", *J. Photon. Technol.*, 17 (2005) 311-314.
[32] W. Xu et al. "Fusion-bonded InSb wafers for photonics networks", *Opt. Res. Lett.*, 22 (2010) 125-128.
[33] Y. Zhang et al. "Room-temperature fusion bonding technology for photonics networks", *Opt. Res. Lett.*, 23 (2011) 103-106.
[34] A. Zahidi et al. "Chemical cleaning of InSb(100) surfaces in HF solutions", *Opt. Mater. Lett.*, 26 (2004) 13-16.
[35] Y. Bond et al. "Chemical cleaning of GaSb(100) surfaces in aqueous solutions", *Opt. Mater. Lett.*, 27 (2005) 215-218.
[36] C. Xiao et al. "SIMS analysis of HF/UV treated silicon (100) surfaces", *Solid Stat. Lett.*, 18 (2019) 69-72.
[37] W. Dillan et al. "Ohmic conduction across wafer-bonded compound semiconducting interfaces", *Acta Mater.*, 22 (2019) 441-444.
[38] E. Varner et al. "Self-propagating low-temperature germanium wafer bonding", *Solid Stat. Lett.*, 21 (2021) 355-358.
[39] U. Fitzgerald et al. "High bonding energy and thermal stress in silicon on ITO wafer bonding", *Solid Stat. Lett.*, 21 (2021) 467-470.
[40] G. Tayeb et al. "Hetero-interface silicon photodetector with high gain-bandwidth-product", *Opt. Res. Lett.*, 32 (2021) 327-330.
[41] S. Hömels et al. "Direct wafer bonding for super-junction fabrication", *Photon. Opto. Lett.*, 19 (2020) 143-146.
[42] I. Reynolds et al. "Non-destructive measurements of wafer-bonded surface energy", *Photon. J. Photon. Technol.*, 31 (2019) 1219-1222.
[43] Q. Jong et al. "Electrical characteristics of CdS/Si heterojunction solar cells under radiation effect", *J. Photon. Technol.*, 25 (2020) 129-132.
[44] K. Poles et al. "Fabrication of CdS/Si heterojunction solar cells by chemical bath method", *Solid Stat. Lett.*, 20 (2020) 277-280.
[45] O. Leon et al. "Deposition of CdSe thin films on ITO substrates by PLD method", *Prog. Mater. Phys.,* 12 (2018) 45-48.
[46] M. Nabawi et al. "Wafer-bonding fabrication of InSb/InP heterostructures on silicon substrates", *Prog. Mater. Phys.,* 13 (2019) 123-126.
[47] N. Müller et al. "Wafer-bonding of InGaP thin films on (100) silicon substrates", *Prog. Mater. Phys.,* 14 (2020) 257-260.
[48] L. Omran et al. "Wafer-bonding of InGaSb thin films on (100) silicon substrates", *Prog. Mater. Phys.,* 15 (2021) 369-372.

